WILEY-VCH

DOI: 10.1002/adfm.201806088
Article type: Full paper

In vivo contactless brain nanothermometry

Blanca del Rosal, Diego Ruiz, Irene Chaves-Coira, Beatriz H. Juárez, Luis Monge, Guosong Hong, Nuria Fernández and Daniel Jaque**

Dr. B. del Rosal
Centre for Micro-Photonics, Faculty of Science, Engineering and Technology, Swinburne University of Technology, Mail H74 PO Box 218, Hawthorn, VIC 3122, Australia

Diego Ruiz, Dr. B. H. Juárez
IMDEA Nanoscience, Faraday 9, Campus Cantoblanco 28049, Madrid, Spain

Dr. I. Chaves-Coira
Department of Anatomy, Histology and Neuroscience, Faculty of Medicine, Universidad Autónoma de Madrid, 28049 Madrid, Spain

Dr. B. H. Juárez
Department of Applied Physical Chemistry, Faculty of Scienceand Condensed Matter Physics Center (IFIMAC)Universidad Autónoma de Madrid, 28049 Madrid, Spain

Prof. L. Monge, Prof. N. Fernández
Fluorescence Imaging Group, Department of Physiology, Faculty of Medicine, Universidad Autónoma de Madrid, 28049 Madrid, Spain
E-Mail: nuria.fernandez@uam.es

Prof. L. Monge, Prof. N. Fernández, Dr. D. Jaque
Instituto Ramón y Cajal de Investigación Sanitaria (IRYCIS), Hospital Ramón y Cajal, 28034 Madrid, Spain

Dr. G. Hong
Department of Chemistry and Chemical Biology, Harvard University, Cambridge, MA 02138, USA

Dr. D. Jaque
Fluorescence Imaging Group, Department of Materials Physics, Faculty of Science, Universidad Autónoma de Madrid, 28049 Madrid, Spain
E-Mail: daniel.jaque@uam.es

Keywords: nanothermometry, infrared bioimaging, transcranial imaging, Ag_2S nanoparticles

https://doi.org/10.1002/adfm.201806088

Despite attracting increased attention from clinicians, brain temperature distribution, fluctuations and changes in response to external stimuli are still largely unknown and refractory to conventional temperature-probing approaches. Fluorescence nanothermometry in the second near-infrared window (NIR-II window, 1,000-1,700 nm), as shown here, can provide contactless brain thermal sensing through the scalp and skull in real time with a sub-degree resolution. As a proof of concept, Ag_2S nanothermometers have been used to monitor brain thermoregulation in a cooling/heating process and temperature changes associated to a barbiturate coma.

https://doi.org/10.1002/adfm.201806088

1. Introduction.

Despite its vital role, the high complexity of the brain makes it the least understood organ. The intrinsic difficulties and limitations of in vivo neuroscience studies further complicate gaining a better understanding of the brain. However, this is essential for developing new approaches that can improve the currently available diagnostic and therapeutic strategies for neurological disorders. Recently, brain temperature distribution and thermal dynamics have emerged as a relevant parameter for brain exploration that can help understand brain physiology and act as a diagnostic indicator.[1] Local temperature in the brain is a vital indicator of neural activity, while modulation of temperature oscillations, such as heating and cooling in local brain regions, enables temporary activation and silencing of neural activities in a transgene-free manner.[2] Research on the physiology of brain temperature changes typically relies on the implantation of invasive probes (thermocouples or fiber optic temperature sensors), which require physical contact with the brain tissue.[3] The relative simplicity of these techniques explains their widespread use in neuroscience research despite their evident limitations, the most important of which is their intrinsic invasiveness. The mismatch of properties between the thermal probes and the brain tissue will result in physical and physiological alterations in the brain, including the formation of glial scars, which prevents their application in long-term experiments. Moreover, the tissue damage that may occur during probe insertion and the heat exchange between the brain tissue and the probe itself can give rise to measurement errors that are hard to quantify.[4] Thermocouples and fiber optic sensors are also limited to point temperature measurements, which complicates studies on brain temperature distribution. Magnetic resonance spectroscopy (MRS), the only currently available technique capable of non-invasive transcranial temperature sensing, allows for brain thermal mapping. The high thermal sensitivity of MRS allows detecting small temperature variations (<1˚C) in the brain, as observed after an ischemia event.[5] MRS

https://doi.org/10.1002/adfm.201806088

overcomes the major limitations of thermocouples and fiber optic sensors for brain temperature sensing, making it a good alternative to invasive probes for experiments in animal models and enabling human experiments. However, the data included in **Table 1**, where we summarize the most relevant parameters of experiments involving real-time brain thermometry, indicate that invasive probes are still the most widespread option in animal research. The high cost of MRS instruments and its limited spatial resolution complicates their application at the small animal level.[6] Measurement artifacts can also arise during MRS brain thermometry due to local variations in tissue magnetic susceptibility values that can impair the accuracy of the temperature reading.[7] Techniques seeking to improve the currently available solutions for brain thermometry at the preclinical level need to overcome their limitations by addressing three main challenges: non-invasiveness, cost-effectiveness and high thermal, spatial and temporal resolution. A contactless approach is key to avoiding damage to the brain tissue and artifacts in the measurements due to tissue-probe interaction, while high sensitivity is needed to record the typically small (< 2˚C, see **Table 1**) brain temperature changes.

As a contactless temperature sensing technique with emerging applications in biomedical research, luminescence nanothermometry can address the challenges described above.[8] This method relies on luminescent nanoparticles (NPs) as thermal reporters and was initially demonstrated for temperature sensing in living cells.[9] The development of luminescent nanothermometers with excitation and emission bands within the near infrared (NIR) expanded their application to living organisms, thanks to the high transparency of tissues in this spectral range.[10] Fluorescent probes emitting in the second NIR window (NIR-II, 1000-1700 nm), where photon scattering by tissues is minimal,[11] enabled transcranial imaging of the cerebral vasculature of mice with a micrometric spatial resolution.[12] The availability of NIR-II luminescent probes (such as Ag_2S and PbS-based NPs)[13] with a temperature-

https://doi.org/10.1002/adfm.201806088

sensitive emission for temperatures in the physiological range enables taking advantage of the high spatial resolution and deep tissue penetration of NIR-II for in vivo thermometry.[14] As the emission of these probes shows a linear and reversible thermal quenching, temperature can be immediately extracted from an intensity analysis of fluorescence images.[15] This has been recently demonstrated in photothermal therapy experiments, where PbS-based QDs provided intratumoral temperature feedback in real time.[16]Preclinical brain research would benefit from the relatively easy implementation and low cost of NIR transcranial temperature sensing as a contactless brain thermometry technique. However, application of NIR-II luminescent nanothermometers for brain thermometry is still an unexplored possibility.

In this work, we employ NIR-II emitting Ag_2S nanodots and a simple NIR small animal imaging setup to achieve transcranial thermal readouts in real time. We have assessed the potential of NIR-II nanothermometry for measuring brain temperature variations in real time through several in vivo experiments, where we have monitored the brain thermal response to different external stimuli and studied its correlation with brain activity.

2. Results and discussion.

For contactless brain thermometry, we envisioned the simple strategy based on the temperature sensitivity of the NIR-II fluorescence emission of Ag_2S nanodots (NDs). **Figure 1** summarizes the most relevant properties of these NDs. Further information about them, including a detailed description of the synthesis procedure, is given in section S1 in the Supporting Information. As shown in the TEM image in **Figure 1(a)**, the Ag_2S NDs used in this work have a spherical shape and an average size of 5 nm (see size histograms in **Figure S2**). The absorption spectrum of an aqueous dispersion of Ag_2S NDs, shown in **Figure 1(b)**, indicates a monotonous increase in the absorbancefor wavelengths below 1000 nm. This allows optical excitation at 808 nm, which is a highly convenient wavelength for in vivo imaging due to the minimal absorption by biological tissues, which translates into high

https://doi.org/10.1002/adfm.201806088

penetration depths with minimal light-induced heating.[17]This wavelength is also convenient from an experimental point of view due to the widespread availability of cost-effective lasers operating at 808 nm. Upon optical excitation at 808 nm, the Ag_2S NDs here used produce a broad emission band centered at 1200 nm, i.e. within the NIR-II window (see **Figure 1(b)**). As previously reported, the fluorescence emission of Ag_2S NDs displays a linear thermal quenching close to room temperature.[18]The thermal quenching observed for water-dispersed NDs also occurs for intracerebrally injected Ag_2S NDs, as shown in **Figure 1(c)**. This figure displays the emission intensity as a function of the brain temperature, as measured ex vivo for Ag_2S NDs allocated inside an excised brain. Experimental details about this calibration given in section S2 in theSupporting Information. To avoid possible misinterpretation of the changes in emission intensity, we verified that the luminescence of the NDs was unaffected by physiological variations in the pH of the brain tissue, as described in section S3 in the Supporting Information.The relative thermal sensitivity of Ag_2S NDs in brain tissue calculated from the linear fitting of the data is included in **Figure 1(d)**.At room temperature, the relative thermal sensitivity of our Ag_2S NDs is close to $3\%\cdot{}^{\circ}C^{-1}$, in good agreement with the value obtained for Ag_2S NDs in other environments (aqueous dispersion and different tissue samples), revealing the robustness of these NDs as nanothermometers.[18] The linear intensity quenchingwith increasing temperature, which originates from the direct relation between temperature and probability of radiative de-excitation,[19] allows remote thermal sensing from a straightforward analysis of infrared fluorescence images.The background noise in the obtained images never exceeded 0.5% of the signal generated by the Ag_2S NDs. Considering the $3\%\cdot{}^{\circ}C^{-1}$ thermal sensitivity of the NDs, this results in an estimated thermal resolution of $\pm$ 0.2 ˚C.

All contactless brain thermometry experiments were performed after intracerebral injection of Ag_2S NDs into CD1 mice following the surgical procedure described insection S4 in the

https://doi.org/10.1002/adfm.201806088

Supporting Information. After injection, the anesthetized mice were illuminated by a fiber-coupled 808 nm diode laser to optically excite the intracerebrally allocated Ag_2S NDs. The experimental setup employed for in vivo image collection is described in detail in section S5 in the Supporting Information. Under our experimental conditions (see section S5), the lateral resolution of the obtained images was ~ 300 μm.We employed time-modulated excitation (100 ms and 500 ms of pulse width and period, respectively)to avoid any possible laser-induced thermal loading due to tissues absorbing a fraction of the laser light. The images were collected with a thermoelectrically cooledInGaAs CCD camera, equipped with an 850 nm longpass filter and NIR focusing optics and synchronized with the excitation laser. The analysis of the NIR-II fluorescence generated by the intracranial Ag_2S NDs provided a remote (contactless) reading of the brain temperature, as schematically represented in **Figure 2(a).Figure 2(b)**shows a representative in vivo fluorescence image obtained through the mouse scalp, in which a bright fluorescent spot at the injection site indicates the presence of intracerebrally injected Ag_2S NDs. The possibility of extracting the brain temperature from a straightforward analysis of the fluorescence intensity generated by the intracerebrally allocated Ag_2S NDs was first demonstrated by monitoring a mouse subjected to a moderate laser-induced heating. We achieved small temperature increases (below 7 ºC at the skin surface) by simply changing the 808 nm time-modulated optical excitation to continuous wave. This causes a moderate laser-induced heating as a consequence of the residual absorption by the fur and the skin.[17, 20] The evolution of the emission of the Ag_2S NDs was monitored during several 4-minute-long irradiation processes. The surface temperature was recorded throughout the experiment with a thermographic camera. **Figure 2(c)** reveals that the brain temperature increment extracted from the NIR images is smaller than that measured at the skin surface. This fact indicates that the heating source in our experimental conditions is located out of cranium. Thus, the observed laser-induced heating stems from the residual

https://doi.org/10.1002/adfm.201806088

absorption of the excitation light by skin and fur, and not from any photothermal heating of the intracerebrally injected Ag_2S NPs or absorption by the brain tissue. Considering the extinction coefficients previously reported at 800 nmforcranial bones (2.2 mm^{-1}) and the average mouse skull thickness (0.4 mm), the optical attenuation of 808 nm radiation when passing through the skull is close to 0.6.[21] This implies that, on average, no more than 40% of the 808 nm excitation light reach the brain, which explains the minimal contribution of the Ag_2S NDs to the overall laser-induced thermal loading observed in our experiments. The normalized temperature vs. time curves measured at the skin and the brain(shown in the inset in **Figure 2(c)**) display identical trends, indicating the unequivocal relationship between the emission of injected Ag_2S NDs and brain temperature. This was corroborated by measurements at different laser power densities in the 0.4-0.9 $W{\cdot}cm^{-2}$ range, as shown in **Figure 2(d)**. As occurs with skin temperature, the brain temperature measured through the emission of Ag_2S NDs increases linearly with increasing laser power density. These results indicate that Ag_2S NDs can measure brain thermal dynamics, yielding results in full agreement with those obtained via conventional infrared thermographic imaging.

Two further experiments were designed to demonstrate the potential of this technique for neuroscience studies. The first of them was an external whole-body cooling experiment (detailed in section S6 in the Supporting Information) to investigate the effects of external thermal stimuli in brain temperature. The mouse was placed in a heating pad throughout the duration of the experiment. The emission of the intracerebrally injected Ag_2S NDs, together with the skin surface temperature and the rectal temperature, was continuously monitored through three distinct experimental stages, as indicated in **Figure 3(a)**. These correspond to thermal stability (region I, heating pad at 33 °C), whole body cooling achieved by cold isopropyl alcohol spraying (region II) and subsequent return to baseline temperature (region III, heating pad at 33 ˚C). The cooling process had a high impact in rectal and skin

https://doi.org/10.1002/adfm.201806088

temperatures, both of which decreased by more than 10 °C showing a similar time evolution. The thermal behavior of the brain, however, was markedly different both in magnitude and time evolution. The magnitude of the brain response to the cooling stimulus, as measured through Ag_2S NDs fluorescence quenching, did not exceed 3 °C. During the thermal relaxation process, brain temperature returned to its baseline value faster than skin and rectal temperatures. This is further evidenced in **Figure 3(b),** where we show the evolution the time derivative of brain and skin temperatures, calculated from data included in Figure 3(a). While the maximum change obtained for brain temperature was close to 0.2 $^{\circ}C \cdot min^{-1}$, the rate of change for skin temperature was much higher, reaching 0.6 $^{\circ}C \cdot min^{-1}$. Data included in **Figure 3** support the previously demonstrated existence of brain thermal regulation mechanisms based in the interplay between cerebral blood flow, cerebrospinal fluid circulation and the thermal impedance provided by both scalp and skull.[5, 22]

Finally, we used Ag_2S NDs to obtain experimental evidence on the strong link between brain temperature and activity. For that purpose, we used Ag_2S NDs for contactless monitoring of brain temperature evolution during a barbiturate coma. Barbiturates can cause a reduction in brain temperature due to their effect on brain metabolism, as has been demonstrated in different animal models.[23]The procedure for intracerebral injection of Ag_2S NDs and NIR-II imaging as well as a full description of the experimental procedure for barbiturate coma induction is given insection S7 in the Supporting Information. Brain temperature and electrical activity were monitored before and after injection of a sodium pentobarbital dose. The time evolution of the brain temperature (**Figure 4(a)**), extracted from the analysis of the NIR-II emission intensity of intracerebrally injected Ag_2S NDs indicates that the pentobarbital injection produces a slight decrease in brain temperature (close to 1 °C). As seen in **Figure 4(b)**, no skin cooling accompanied the observed brain cooling, indicating its direct association with barbiturate-induced decrease in brain metabolic activity. The

https://doi.org/10.1002/adfm.201806088

administrated sodium pentobarbital dose elicited a burst-suppression electroencephalographic pattern with a progressive reduction in the amplitude of the electroencephalography (EEG) waves until an isoelectric state was reached, as shown in **Figures 4(c)-(e)**. Results in **Figure 4** indicate that an immediate temperature decrease accompanies the suppression in electrical activity caused by the pentobarbital injection. Brain cooling, therefore, occurs as a consequence of the drug-induced reduction in brain activity and metabolism as it had been previously postulated.[23]The magnitude of the change in brain temperature induced by the sodium pentobarbital dose measured here is in good agreement with the magnitude of previously reported drug-induced brain temperature changes in animal models (see **Table 1**).

3. Conclusions.

In summary, this work presents a simple method for contactless brain thermometry in real time for accurate and real-time measurement of brain activity in murine models. Temperature-sensitive Ag_2S NDs enable brain thermal sensing through a straightforward analysis of NIR fluorescence images. We have demonstrated the capability of our experimental approach in two proof-of-concept experiments. The existence of brain thermoregulation mechanisms has been evidenced by its thermal response to an external cooling stimulus. Furthermore, in a barbiturate-induced coma, we have shown that the suppression in brain activity is accompanied by a slight temperature reduction.

NIR-II nanothermometry, as shown in this work, offers the possibility of contactless, minimally invasive brain temperature sensing in real time. This would, in turn, contribute to gaining a better understanding of brain dynamics involved in a variety of pathological conditions, including non-invasive monitoring and treatment of epileptic seizure, traumatic brain injury and stroke. In addition, the close correlation between local neural activity and temperature variations makes the contactless deep-brain nanothermometry a valuable approach to interrogate brain activity in a non-invasive manner.

https://doi.org/10.1002/adfm.201806088

Experimental Section

Experimental details are given in the Supporting Information.

Supporting Information

Supporting Information is available from the Wiley Online Library or from the author.

Acknowledgements

Work supported by the Spanish Ministry of Economy and Competitiveness under Projects # MAT2016-75362-C3-1-R and #FIS2015-67367-C2-1-P, and from and by Instituto de Salud Carlos III under Project # PI16/00812. COST Action CM1403 and UAM-Santander Yerun Projects are also acknowledged. This work has also received support from ComunidadAutónoma de Madrid (B2017/BMD-3867RENIM-CM and S2013/MIT-2740) and the European Commission (NanoTBTech). Work cofinanced with Structural Funds from the European Union.BHJ acknowledges financial support from the Spanish Ministry of Economy and Competitiveness, through the "Maria de Maeztu" (IFIMAC) and "Severo Ochoa" (IMDEA Nanoscience) Programmes for Units of Excellence in R&D.

Received: ((will be filled in by the editorial staff))
Revised: ((will be filled in by the editorial staff))
Published online: ((will be filled in by the editorial staff))

https://doi.org/10.1002/adfm.201806088

References

[1] a) H. Wang, B. Wang, K. P. Normoyle, K. Jackson, K. Spitler, M. F. Sharrock, C. M. Miller, C. Best, D. Llano, R. Du, *Front. Neurosci.***2014**, 8, 307;b) R. A. Bola, E. A. Kiyatkin, *Neuropharmacology***2017**, 126, 271.

[2] a) R. Chen, G. Romero, M. G. Christiansen, A. Mohr, P. Anikeeva, *Science***2015**, 347, 1477;b) J.-M. Ramirez, L. P. Folkow, A. S. Blix, *Annu. Rev. Physiol.***2007**, 69, 113.

[3] a) S. Musolino, E. P. Schartner, G. Tsiminis, A. Salem, T. M. Monro, M. R. Hutchinson, *Biomed. Opt. Express* **2016**, 7, 3069;b) Y. Takeda, H. Hashimoto, K. Fumoto, T. Danura, H. Naito, N. Morimoto, H. Katayama, S. Fushimi, A. Matsukawa, A. Ohtsuka, K. Morita, *Anesthesiology***2012**, 117, 117.

[4] R. Chen, A. Canales, P. Anikeeva, *Nat. Rev. Mater.* **2017**, 2, 16093.

[5] B. Karaszewski, J. M. Wardlaw, I. Marshall, V. Cvoro, K. Wartolowska, K. Haga, P. A. Armitage, M. E. Bastin, M. S. Dennis, *Ann. Neurol.***2006**, 60, 438.

[6] a) V. Rieke, K. Butts Pauly, *J. Magn. Reson. Imaging***2008**, 27, 376;b) X.-F. Yang, J. H. Chang, S. M. Rothman, *Epilepsy Research***2002**, 52, 97.

[7] S. Onitsuka, D. Nakamura, T. Onishi, T. Arimitsu, H. Takahashi, H. Hasegawa, *Sci. Rep.***2018**, 8, 2757.

[8] a) C. D. S. Brites, P. P. Lima, N. J. O. Silva, A. Millan, V. S. Amaral, F. Palacio, L. D. Carlos, *Nanoscale***2012**, 4, 4799;b) M. Quintanilla, L. M. Liz-Marzán, *Nano Today***2018**.

[9] a) D. Jaque, B. d. Rosal, E. M. Rodríguez, L. M. Maestro, P. Haro-González, J. G. Solé, *Nanomedicine***2014**, 9, 1047;b) C. F. Chapman, Y. Liu, G. J. Sonek, B. J. Tromberg, *Photochem. Photobiol.***1995**, 62, 416;c) J. S. Donner, S. A. Thompson, M. P. Kreuzer, G. Baffou, R. Quidant, *Nano Lett.***2012**, 12, 2107;d) K. Okabe, N. Inada, C. Gota, Y. Harada, T. Funatsu, S. Uchiyama, *Nat. Commun.***2012**, 3, 705.

[10] a) B. del Rosal, E. Ximendes, U. Rocha, D. Jaque, *Adv. Opt. Mater.***2016**, 5, 1600508;b) M. Xu, X. Zou, Q. Su, W. Yuan, C. Cao, Q. Wang, X. Zhu, W. Feng, F. Li, *Nat. Commun.***2018**, 9;c) R. R. Anderson, J. A. Parrish, *J. Invest. Dermatol.***1981**, 77, 13;d) G. Hong, A. L. Antaris, H. Dai, *Nat. Biomed. Eng.***2017**, 1, 0010.

[11] a) A. M. Smith, M. C. Mancini, S. Nie, *Nat. Nanotechnol.***2009**, 4, 710;b) G. Hong, J. C. Lee, J. T. Robinson, U. Raaz, L. Xie, N. F. Huang, J. P. Cooke, H. Dai, *Nat. Med.***2012**, 18, 1841.

[12] G. Hong, S. Diao, J. Chang, A. L. Antaris, C. Chen, B. Zhang, S. Zhao, D. N. Atochin, P. L. Huang, K. I. Andreasson, C. J. Kuo, H. Dai, *Nat. Photonics***2014**, 8, 723.

[13] a) Y. Zhang, G. Hong, Y. Zhang, G. Chen, F. Li, H. Dai, Q. Wang, *ACS Nano***2012**, 6, 3695;b) A. Benayas, F. Ren, E. Carrasco, V. Marzal, B. del Rosal, B. A. Gonfa, Á. Juarranz, F. Sanz‐Rodríguez, D. Jaque, J. García‐Solé, *Adv. Funct. Mater.***2015**, 25, 6650.

[14] E. Hemmer, A. Benayas, F. Legare, F. Vetrone, *Nanoscale Horiz.***2016**, 1, 168.

[15] E. C. Ximendes, U. Rocha, T. O. Sales, N. Fernández, F. Sanz‐Rodríguez, I. R. Martín, C. Jacinto, D. Jaque, *Adv. Funct. Mater.***2017**, 27, 1702249.

[16] B. del Rosal, E. Carrasco, F. Ren, A. Benayas, F. Vetrone, F. Sanz‐Rodríguez, D. Ma, Á. Juarranz, D. Jaque, *Adv. Funct. Mater.***2016**, 26, 6060.

[17] L. M. Maestro, P. Haro-González, B. Del Rosal, J. Ramiro, A. Caamano, E. Carrasco, A. Juarranz, F. Sanz-Rodríguez, J. G. Solé, D. Jaque, *Nanoscale***2013**, 5, 7882.

[18] D. Ruiz, B. del Rosal, M. Acebrón, C. Palencia, C. Sun, J. Cabanillas‐González, M. López-Haro, A. B. Hungría, D. Jaque, B. H. Juarez, *Adv. Funct. Mater.***2017**, 27, 1604629.

https://doi.org/10.1002/adfm.201806088

[19] H. Santos, D. Ruiz, G. Lifante, C. Jacinto, B. Juarez, D. Jaque, *Nanoscale***2017**, 9, 2505.
[20] B. del Rosal, I. Villa, D. Jaque, F. Sanz-Rodríguez, *J. Biophotonics***2016**, 9, 1059.
[21] a) H. Soleimanzad, H. Gurden, F. Pain, *J. Biomed. Opt.***2017**, 22, 010503;b) E. A. Genina, A. N. Bashkatov, V. V. Tuchin, *Advances in Optical Technologies***2008**, 2008;c) A. N. Bashkatov, E. A. Genina, V. I. Kochubey, V. V. Tuchin, presented atSaratov Fall Meeting 2005: Optical Technologies in Biophysics and Medicine VII **2006**.
[22] H. Wang, M. Kim, K. P. Normoyle, D. Llano, *Front. Neurosci.***2015**, 9, 528.
[23] E. A. Kiyatkin, P. L. Brown, *Physiol. Behav.***2005**, 84, 563.
[24] A. R. Laptook, R. J. T. Corbett, R. Sterett, D. Garcia, G. Tollefsbol, *Pediatr. Res.***1995**, 38, 919.
[25] M. Caiazzo, M. T. Dell'Anno, E. Dvoretskova, D. Lazarevic, S. Taverna, D. Leo, T. D. Sotnikova, A. Menegon, P. Roncaglia, G. Colciago, *Nature***2011**, 476, 224.
[26] M. Bejanian, B. L. Jones, P. J. Syapin, D. A. Finn, R. L. Alkana, *Pharmacology Biochemistry and Behavior***1991**, 39, 457.
[27] M. O. Baud, P. J. Magistretti, J.-M. Petit, *Journal Of Sleep Research***2013**, 22, 3.
[28] E. A. Kiyatkin, P. L. Brown, R. A. Wise, *European Journal of Neuroscience***2002**, 16, 164.
[29] I. V. Yekimova, I. Pastukhov, *Doklady biological sciences: proceedings of the Academy of Sciences of the USSR, Biological sciences sections / translated from Russian***2002**, 387, 485.

https://doi.org/10.1002/adfm.201806088

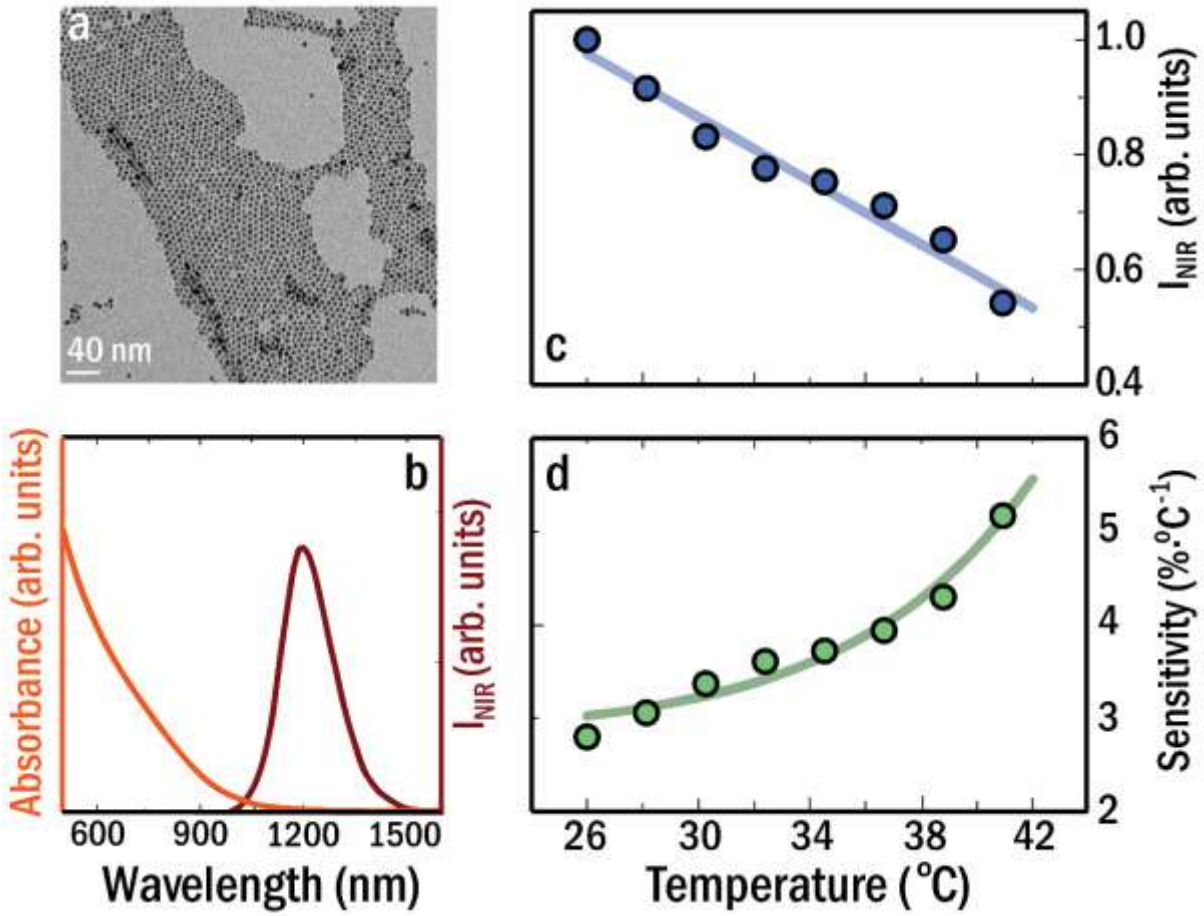

Figure 1.- Characterization of Ag_2S NDs **(a)** Representative TEM image of the Ag_2SNDs used in this work. **(b)** Room temperature absorption and emission spectra of an aqueous dispersion of Ag_2SNDs in PBS. The excitation wavelength (808 nm) used in this work is also indicated in the figure. **(c)** Temperature dependence of the fluorescence intensity generated by Ag_2S NDs. The linear calibration curve allows for direct contactless brain temperature measurement from the analysis of fluorescence intensities in the NIR-II images with a relative thermal sensitivity shown in **(d)**. The dots in (c) and (d) correspond to the experimental data and the lines are included as guides for the eyes.

https://doi.org/10.1002/adfm.201806088

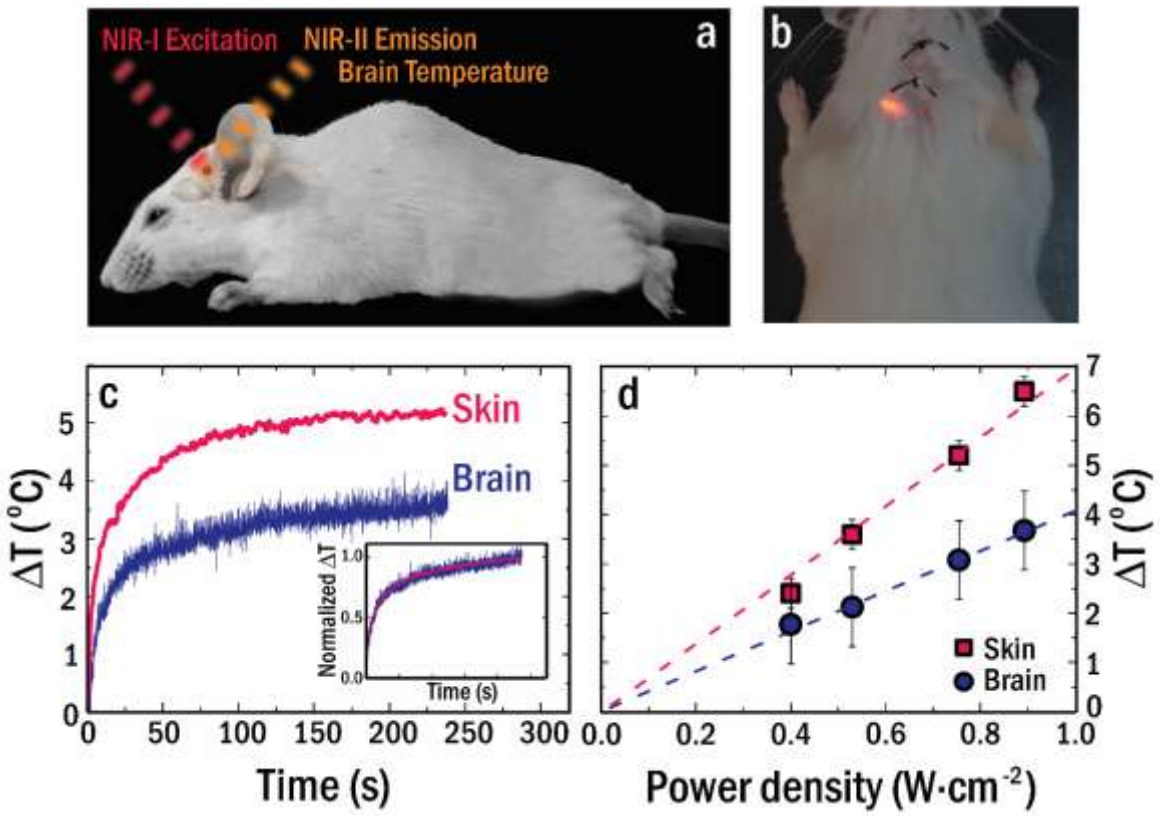

Figure 2.- Principle of contactless brain temperature measurements by luminescence nanothermometry. **(a)** Schematic diagram of the operation principle. Intracerebrally injected Ag_2S nanodots (NDs) act as thermal reporters. Under 808 nm pulsed optical excitation, Ag_2S NDs produce an intense NIR-II fluorescence. The real time analysis of the luminescence intensity provides remote temperature reading. **(b)** Representative in vivo infrared fluorescence image, merged with an optical image of the mouse under investigation, revealing the presence of intracerebrally injected Ag_2S NDs. **(c)**Temperature change at the skin surface (measured by infrared thermography) and the brain (measured by Ag_2S NDs NIR-II fluorescence) during a 4-minute-long exposure to 808 nm laser light (0.78 $W \cdot cm^{-2}$). The inset shows the normalized curves, where the identical trend followed by skin and brain temperature changes is evidenced. **(d)**Temperature change at the skin surface and the brain for 4-minute long exposures to 808 nm laser light at different power densities.

https://doi.org/10.1002/adfm.201806088

WILEY-VCH

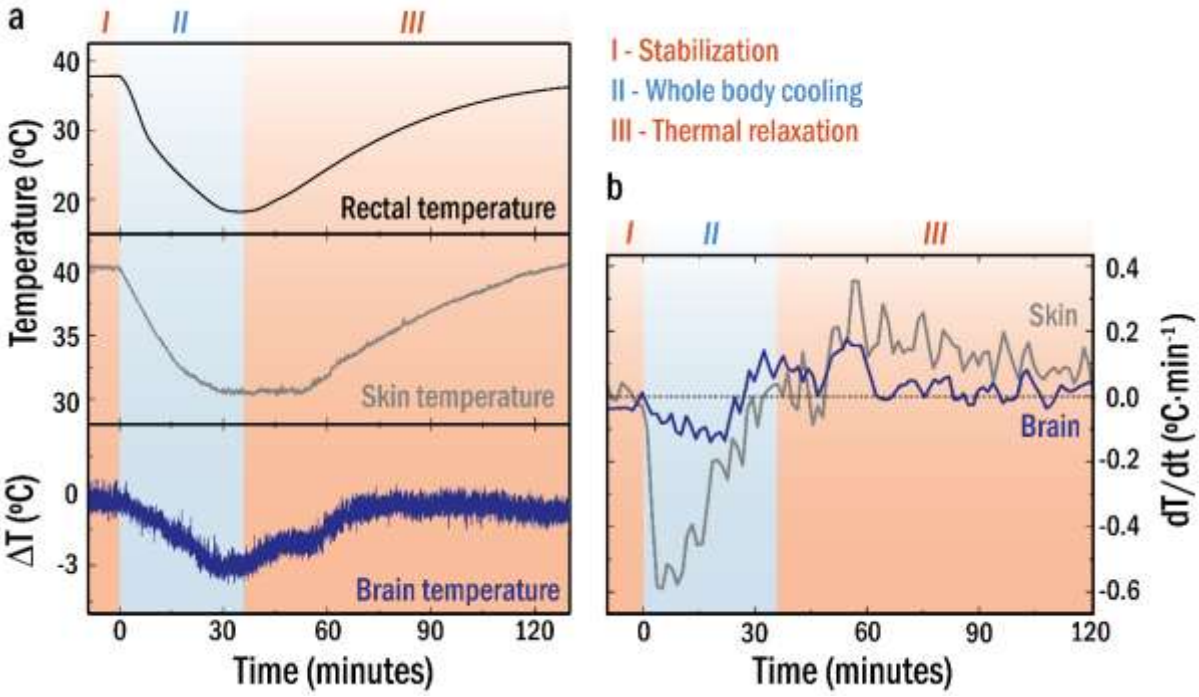

Figure 3.-Contactless in vivo brain thermometry by Ag_2S NDs during a whole body cooling/heating process. **(a)** Time evolution of rectal, skin and brain temperature during a whole body cooling experiment. I, II and III correspond to the different stages of the experiment: thermal stability, cooling and subsequent thermal relaxation, respectively. **(b)** Evolution of the time derivate of both brain and skin temperatures as obtained from the experimental data included in **(a)**.

https://doi.org/10.1002/adfm.201806088

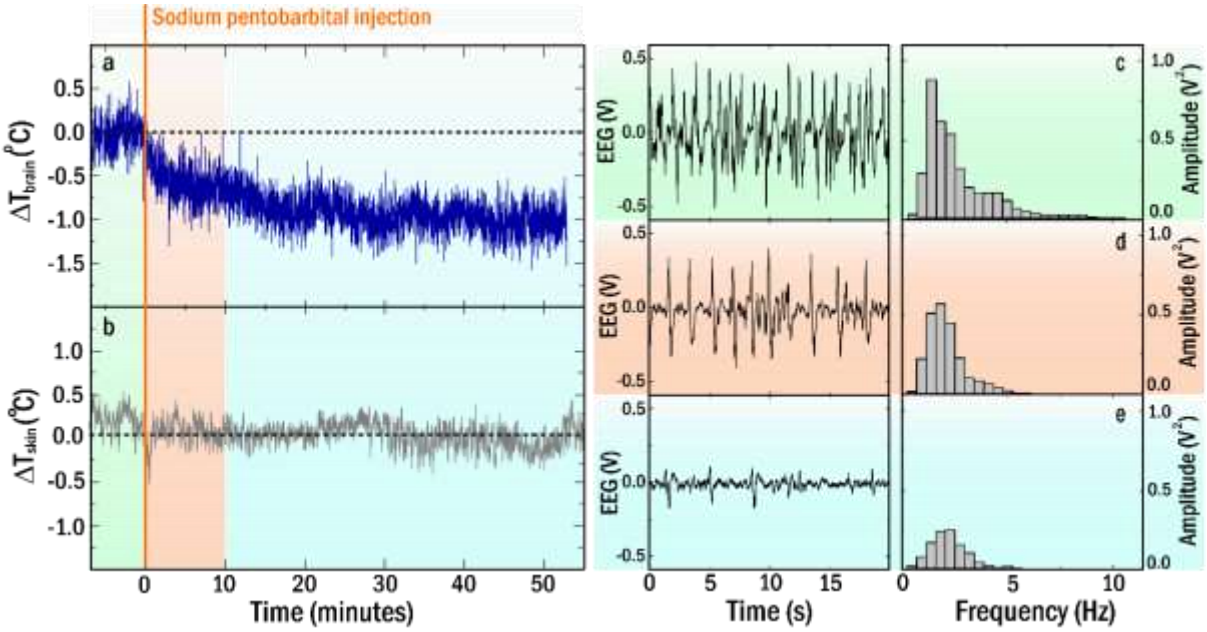

Figure 4.- Contactless brain thermometry by Ag_2S NDs during barbiturate-induced coma. **(a)-(b)** Temperature change induced by the administration of a sodium pentobarbital dose at the time indicated by the vertical solid line (a) in the brain and (b) at the skin. Dashed horizontal lines indicate the basal temperature values. **(c)-(e)** Electroencephalography (EEG) patterns obtained at different times before (c) or after (d, e) sodium pentobarbital injection. The barbiturate-induced reduction in electrical activity at the brain accompanies the experimentally observed reduction in brain temperature.

https://doi.org/10.1002/adfm.201806088

Stimulus	Animal model	ΔT_{brain} (˚C)	Time scale	Method	Contact	Ref.
Drug administration (heroine)	Rats	+1.2	0-40 min	Implanted thermocouples	YES	[1b]
Hypoxia	Hooded seals	-3	0-20 min	Implanted thermocouples	YES	[2b]
Drug administration (4-AP)	Rats	+0.4	0-30 s	Implanted thermocouples	YES	[6b]
Cardiac arrest	Monkeys	-1	0-12 min	Implanted thermocouples	YES	[3b]
Ischemia	Humans	+0.4	Days	Magnetic resonance spectroscopy	NO	[5]
Ice slurry ingestion	Humans	-0.4	0-25 min	Magnetic resonance spectroscopy	NO	[7]
Ischemia	Piglets	+10	NA	Magnetic resonance spectroscopy	NO	[24]
Microwave heating	Rats	+2	NA	Thermal sensor implantation	YES	[25]
Ethanol administration	Mice	-2	0-10 min	Thermal sensor implantation	YES	[26]
Sleep	Mice	-1.2	0-10 hours	Thermal sensor implantation	YES	[27]
Drug administration (Pentobarbital)	Rats	-1.2	0-80 min	Implanted thermocouples	YES	[23]
Tail pinch	Rats	+1	0-10 min	Implanted thermocouples	YES	[28]
Unexpected sound	Rats	+0.25	0-4 min	Implanted thermocouples	YES	[28]
Drug administration (muscimol)	Pigeons	-1.5	0-1 hours	Implanted thermocouples	YES	[29]
Saline injection	Rats	-0.75	0-100 min	Implanted optical fibers	YES	[3a]
Whole body cooling	Mice	-3	0-30 min	Luminescence nanothermometry	NO	This work
Drug administration (Pentobarbital)	Mice	-1	0-30 min	Luminescence nanothermometry	NO	This work
Laser heating	Mice	+4	0-3 min	Luminescence nanothermometry	NO	This work

Table 1.- Summary of the relevant parameters of experimental works dealing with in vivo brain thermometry in different animal models and humans. The stimulus used to provoke the temperature change, the animal model, the magnitude and time scale of the temperature change, and the thermometry technique are indicated in each case. The existence of physical contact between brain and thermal sensor is also indicated.

https://doi.org/10.1002/adfm.201806088

WILEY-VCH

The thermal sensitivity of infrared-emitting Ag_2S nanodots enables in vivo, real-time contactless brain thermometry. The lack of techniques for continuous, minimally invasive probing of brain temperature has complicated its study despite its relevance in brain physiology and pathology. Luminescence nanothermometry overcomes this limitation, as is here demonstrated by live tracking of drug-induced brain temperature changes and their link to neural activity.

Nanothermometry

B. del Rosal, D. Ruiz, I. Chaves-Coira, B. H. Juárez, L. Monge, G. Hong, N. Fernández, D. Jaque*

In vivo contactless brain nanothermometry

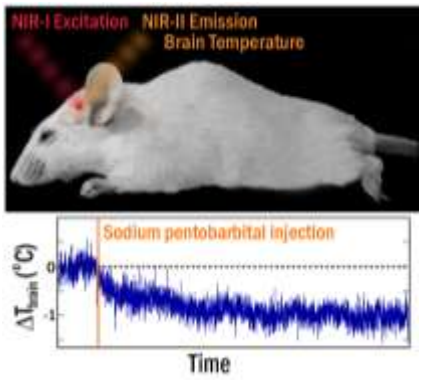

https://doi.org/10.1002/adfm.201806088